

Thermophysical Property Measurements: Improved Density, Viscosity and Thermal Diffusivity Methods

Chemical and Fuel Cycle Technologies Division

About Argonne National Laboratory

Argonne is a U.S. Department of Energy laboratory managed by UChicago Argonne, LLC under contract DE-AC02-06CH11357. The Laboratory's main facility is outside Chicago, at 9700 South Cass Avenue, Argonne, Illinois 60439. For information about Argonne and its pioneering science and technology programs, see www.anl.gov.

DOCUMENT AVAILABILITY

Online Access: U.S. Department of Energy (DOE) reports produced after 1991 and a growing number of pre-1991 documents are available free at OSTI.GOV (<http://www.osti.gov/>), a service of the US Dept. of Energy's Office of Scientific and Technical Information.

Reports not in digital format may be purchased by the public from the National Technical Information Service (NTIS):

U.S. Department of Commerce
National Technical Information Service
5301 Shawnee Rd
Alexandria, VA 22312
www.ntis.gov
Phone: (800) 553-NTIS (6847) or (703) 605-6000
Fax: (703) 605-6900
Email: **orders@ntis.gov**

Reports not in digital format are available to DOE and DOE contractors from the Office of Scientific and Technical Information (OSTI):

U.S. Department of Energy
Office of Scientific and Technical Information
P.O. Box 62
Oak Ridge, TN 37831-0062
www.osti.gov
Phone: (865) 576-8401
Fax: (865) 576-5728
Email: **reports@osti.gov**

Disclaimer

This report was prepared as an account of work sponsored by an agency of the United States Government. Neither the United States Government nor any agency thereof, nor UChicago Argonne, LLC, nor any of their employees or officers, makes any warranty, express or implied, or assumes any legal liability or responsibility for the accuracy, completeness, or usefulness of any information, apparatus, product, or process disclosed, or represents that its use would not infringe privately owned rights. Reference herein to any specific commercial product, process, or service by trade name, trademark, manufacturer, or otherwise, does not necessarily constitute or imply its endorsement, recommendation, or favoring by the United States Government or any agency thereof. The views and opinions of document authors expressed herein do not necessarily state or reflect those of the United States Government or any agency thereof, Argonne National Laboratory, or UChicago Argonne, LLC.

Thermophysical Property Measurements: Improved Density, Viscosity and Thermal Diffusivity Methods

by

M.A. Rose, E. Wu, and M.A. Williamson

Chemical and Fuel Cycle Technologies Division, Argonne National Laboratory

November 16, 2020

CONTENTS

1.	Introduction	1
2.	Source Materials and Salt Preparation	1
3.	Density.....	3
3.1	Density Measurement Method	4
3.2	Density Measurements of Eutectic FLiNaK	6
3.3	Discussion of Density Measurements	8
4.	Viscosity	9
4.1	Viscosity Measurement Method.....	9
4.2	Viscosity Measurements of Eutectic FLiNaK.....	11
4.3	Improved Viscosity Measurement Protocol.....	13
5.	Thermal Diffusivity.....	15
5.1	Thermal Diffusivity Measurement Method.....	15
5.2	Thermal Diffusivity of Graphite.....	17
5.3	Thermal Diffusivity Measurements of Eutectic FLiNaK.....	20
6.	Summary	21
	Acknowledgement.....	22
	References	23

1. Introduction

The technical bases and methods developed at Argonne to measure thermophysical properties of molten salt mixtures are summarized and representative results provided to show the accuracy and precision achieved. Three key measurements addressed in this report are density, viscosity and thermal diffusivity. The densities of two eutectic FLiNaK mixtures were measured at temperatures to approximately 750 °C and the results are compared with literature values. The results are used to show how the effect of salt surface tension is taken into account in the density calculation and how the surface tension for other salt mixtures is being measured. Viscosity measurements of eutectic FLiNaK are shown to illustrate improvements to the measurement method being made to address and minimize the sources of error and uncertainties in the reported values. Thermal diffusivity measurements of FLiNaK are shown to illustrate the measurement method developed at Argonne and the achieved precision. The thermal diffusivity of the graphite used to make the cells that contain the salts during analyses was measured to assess the relative contribution to the response. The improved procedures developed in this work are being applied in property measurements of other salts of interest.

2. Source Materials and Salt Preparation

The reagents used to prepare salt mixtures for measurements are purchased at the highest purities available (better than 99.9% by trace metals analysis) and analyzed before use. Appendix A contains material certificates for representative salt reagents provided by the manufacturers. Salt mixtures and samples to be analyzed are prepared in argon atmosphere gloveboxes in which oxygen and moisture levels are maintained below 10 ppm. Reagent salts are characterized by using powder X-ray diffraction prior to use to confirm the compositions and detect significant amounts of impurities. Samples are fixed onto slides with double-sided tape and sealed with Kapton® polymer film while inside the glovebox to avoid contamination throughout the analysis. A Bruker D5000 X-ray diffraction (XRD) system is used to measure the pattern over the range $2\theta = 10^\circ$ to 100° . Figure 1 shows the measured XRD diffraction patterns for LiF, KF, and NaF reagents. The circles indicate the intensities and locations of peaks listed in the International Center for Diffraction Data database that were used to confirm the identities of the reagent salts. The compositions of all reagents were confirmed.

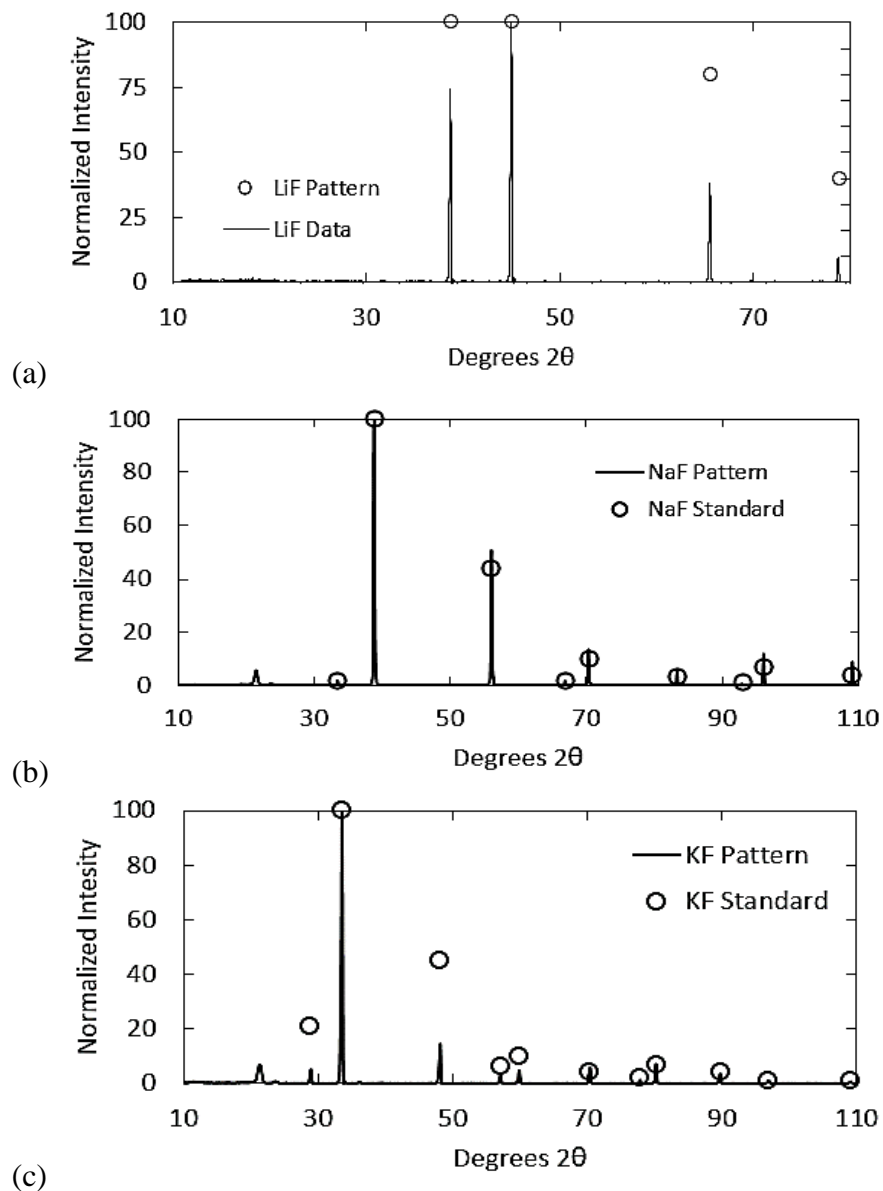


Figure 1. Measured X-ray Diffraction Patterns and Literature Data for Reagent Salts (a) LiF, (b) NaF, and (c) KF

Salt mixtures are typically prepared by placing the appropriate amounts of reagent salts in a Ni crucible and heating twice in a furnace to melt and homogenize the material. The Ni crucible is manually polished with steel wool prior to use – to remove any oxide residue and prevent oxide contamination of the mixtures. The fused salt is ground to a fine powder after each heating by using a mortar and pestle. The mortar and pestles are cleaned with methanol after each use. Separate mixtures of eutectic FLiNaK prepared in 2019 and 2020 were used for the density measurements discussed in this report and are referred to by the year of their production, to assess

the effect of minor composition differences in the measured values. Details on their production are available in previous reports [1, 2]. Viscosity and thermal diffusivity measurements were made with separately batched mixtures of eutectic FLiNaK. Major element analyses of the salts by using inductively coupled plasma-optical emission spectroscopy (ICP-OES) are shown for all the eutectic FLiNaK mixtures in Table 1. This technique is typically accurate to 10% of the reported values. The uncertainty listed in the table is one standard deviation of the values measured for replicate samples. Only one analysis of the 2019 mixture used for density measurements was made.

Table 1. Major Element Analysis by ICP-OES of FLiNaK by Measurement, in mol %

Batched for	NaF	KF	LiF
2019-Density	11.1	41.8	47.1
2020-Density	11.5 ± 0.2	42.0 ± 0.6	46.5 ± 0.5
Thermal Diffusivity	11.6 ± 0.6	41 ± 2	47 ± 2
Viscosity	11.4 ± 0.6	42 ± 2	46 ± 2

Inductively coupled plasma-mass spectroscopy (ICP-MS) was used to measure trace element concentrations in the salts used to measure density. The results of those analyses are shown in Table 2. The higher concentration of calcium in the 2020 eutectic FLiNaK is contamination from the large ceramic mortar and pestle used to grind that salt to a powder. The much smaller volume of salt made in 2019 salt was ground in an agate mortar and pestle and did not have significant calcium contamination. Grinding large volumes of salts will be done using a high capacity automated stainless steel mortar and pestle in the future to prevent calcium contamination.

Table 2. Trace Element Analysis by ICP-MS of FLiNaK for Density Measurements, in ppm

Salt Batch	Mg	Ca	Cr	Mn	Fe	Ni	Rb	Cs
2019	24	76	6	3	117	179	44	2
2020	BDL	981 ± 490	BDL	BDL	BDL	123 ± 12	28.0 ± 3.4	1.8 ± 0.4

3. Density

Knowing the salt density over the full operational range of a molten salt reactor (MSR), including changes that occur as the fission products and contaminants accumulate, is crucial for design and safety assessments. Establishing a standard procedure and reference salt composition for measuring density of molten salts with known precision will allow measurements to be validated across laboratories to provide data with the appropriate quality for use in design and safety assessments. Eutectic FLiNaK is a commonly used salt that may be suitable for use as a reference material to establish expected property values and measurement precision.

3.1 Density Measurement Method

Density was determined by using a displacement method based on the Archimedes principle, which states that the buoyant force on an object is equal to the weight of the liquid it displaces. This principle can be used to calculate the density of a liquid by comparing the weight of a solid bob of known mass and volume in a gas space and the mass measured when the bob is immersed in the liquid. Equation 1 relates the fluid density to the difference in the masses of the bob measured in air (or the glovebox atmosphere) and immersed in the molten salt and takes the effects of the thermal expansion of the bob (α) and the surface tension (σ) of the liquid into account [6].

$$\rho = \frac{\Delta m + \frac{\pi D \sigma}{g}}{V_0 [1 + \alpha T]^3} \quad (1)$$

Here, D is the diameter of the bob, V_0 is the volume of the bob, and T is the temperature of the molten salt in Kelvin. The surface tension of the salt can be determined by making measurements using two different size wires and bobs. Separate measurements were made using 0.25 mm and 0.5 mm diameter wires and 2 cm³ and 1 cm³ sized bobs to determine the effect of the surface tension on the calculated density. The surface tension of FLiNaK was calculated using a correlation from the literature [10] shown in Equation 2.

$$\sigma \text{ (N m}^{-1}\text{)} = 0.2726 - 1.014 \times 10^{-4} T \text{ (K)} \quad (2)$$

The effect of thermal expansion is minimized by using a Ni bob that has a low thermal expansion coefficient. The linear thermal expansion coefficient of nickel is $13.0 \times 10^{-6} \text{ K}^{-1}$. A photo of a Ni bob used in the density measurements is shown in Figure 2. A new bob was used in each series of measurements to prevent cross contamination between salts.



Figure 2. Photograph of Ni Bob used in Density Measurements

The apparatus used at Argonne consists of a balance placed on an XY linear stage on top of a scissor lift. A drawing of the test apparatus used to measure molten salt density is provided in Figure 3. The balance is carefully positioned above a furnace well containing the molten salt and

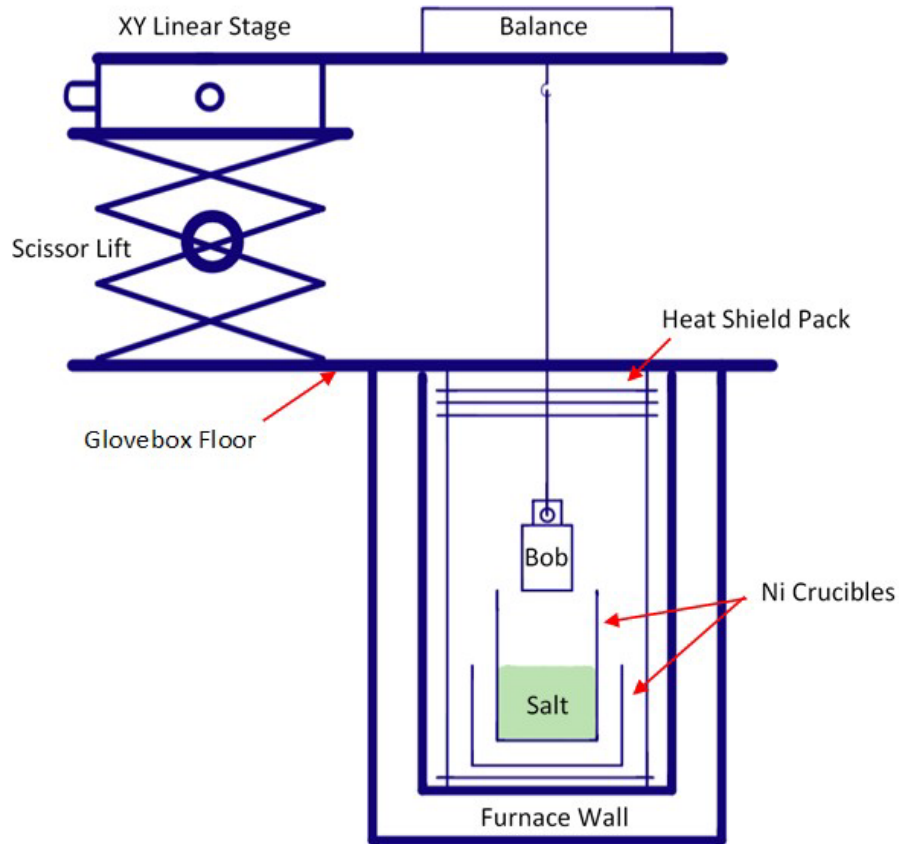


Figure 3. Schematic of the Density Measuring Device

the bob is suspended by a wire hung from the underweighing hook on the balance. The stand holding the balance is moved up and down to raise and lower the bob out of and into the molten salt.

Salt is contained in a nickel crucible that is nested inside a second nickel crucible, which is used to collect any overflow of salt when the bob is immersed. Both crucibles are polished with steel wool, to remove oxides before use, after being placed in the glovebox. Salt is placed in the inner nickel crucible and heated for 20 hours before measurements are made. After immersion, the bob is allowed to thermally equilibrate with the salt for at least two hours. Data are taken for approximately 10-15 minutes at each stable temperature. Measurements are made at approximately 50 °C intervals over the temperature range of interest and the melt and bob are allowed to thermally equilibrate for more than two hours after the temperature is changed between measurements.

The change in density caused by a temperature difference (ΔT) of a fixed mass of salt is given by the volumetric thermal expansion coefficient of the salt. The volumetric thermal expansion coefficient, β , of each fuel salt can be calculated using Equation 3, where ρ_0 and ρ_1 are the densities determined at two temperatures.

$$\rho_1 = \frac{\rho_0}{(1-\beta\Delta T)} \quad (3)$$

3.2 Density Measurements of Eutectic FLiNaK

The densities of separate batches of eutectic FLiNaK were measured in 2019 and 2020 at temperatures from 600 to 750 °C. Densities were measured in separate series at descending salt temperatures and after random changes in the salt temperature in 2019 and at ascending temperatures in 2020. The submerged masses of the nickel bob in these measurements are recorded in Appendix Table B.1-3 and used to calculate the salt densities by using Equation 1. Note that all densities were calculated including the surface tension term in Equation 1. The volume of the bobs were calculated from their weights in the glovebox atmosphere using the density of nickel (8.908 g mL⁻¹).

The densities at different temperatures, and measured in different orders, are summarized in Figure 4. Densities calculated from measurements made at descending temperatures (circles), measurements made at randomly ordered temperatures (triangles), and measurements made at ascending temperatures (diamond) are in good agreement. In Figure 4, the uncertainty in the measured masses in 2019 was ± 0.0003 g and the corresponding uncertainty in the density was ± 0.0006 g cm⁻³ at all temperatures. The uncertainty in the masses measured in 2020 was ± 0.025 g and the uncertainty of the density was 0.01 g cm⁻³ at all temperatures. Small differences in 2019 and 2020 results could be due to small differences in the compositions of the two batches of FLiNaK salt, which are listed in Table 1 [1, 2].

The higher standard deviation in the densities of FLiNaK measured in 2020 compared to those measured in 2019 is attributed to a change in experimental apparatus. The balance and support system was moved to a different glovebox prior to the measurements made in 2020 to enable work with greater quantities of radioactive materials. The furnace used in that glovebox did not maintain temperature as accurately as the furnace that had been used in the other glovebox. Using the new furnace, the salt temperature was observed to cycle over a 6 °C range and the measured mass varied by a maximum of 100 mg in response to the temperature changes during all measurements. Measurements were made for sufficient durations that the average values of the measured temperature and mass are reliable despite the variance in the data sets. The furnace has recently been modified to improve the level of temperature control, but these results show that a high degree of temperature stability is essential to achieving low uncertainty in the density measurements.

Despite the variance due to the temperature instability, the average values of densities measured during 2020 are in excellent agreement with densities measured during 2019. A trend line fit to the pooled results is shown in Figure 4. Using this trend line and Equation 3, a volumetric thermal expansion coefficient of $\beta = -3.03 \times 10^{-4}$ K⁻¹ was calculated over the temperature range of the measurements.

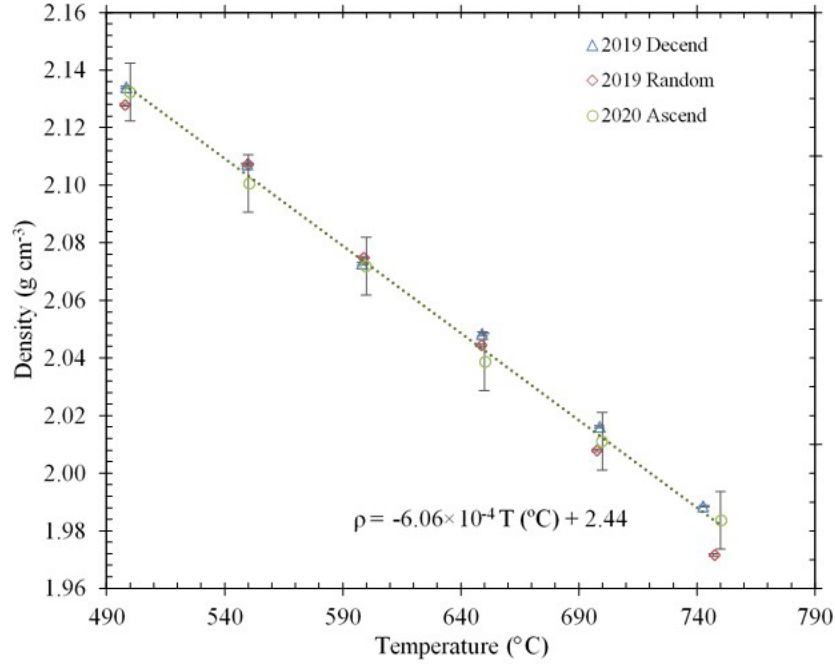


Figure 4. Measured Density of FLiNaK at Argonne at Different Temperature Orders

The importance of the surface tension term in the density calculation is illustrated in Figure 5, where the density values shown in the left figure have been calculated by using Equation 1, but neglecting the surface tension term. The density values in the figure on the right were calculated with the surface tension term using the diameters of the wire and surface tension values from the literature (as were the values plotted in Figure 4). The contribution of the surface tension term on

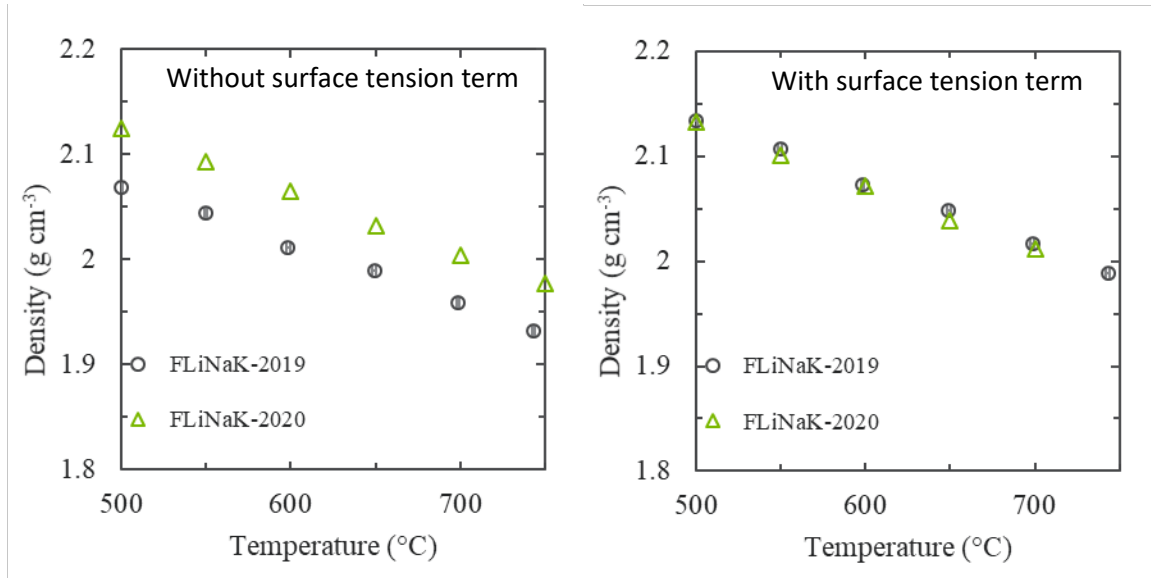


Figure 5. 2019 and 2020 Density Measurements of Eutectic FLiNaK Neglecting Surface Tension Term (left) and Using a Surface Tension Value from Literature (Right)

the 2019 measurements is 8–10 times greater than the contribution in the 2020 density measurements because a smaller bob and a thicker leading wire were used for measurements in 2019. The masses of the bobs and the diameters of the wires used in the measurements made in 2019 and in 2020 are summarized in Table 3.

Table 3. Bob Mass and Leading Wire Diameter for FLiNaK Density Measurement

	Bob Mass (g)	Bob Volume (cm³)	Wire Diameter (mm)
2019	4.21	0.472	0.50
2020	18.48	2.075	0.25

It is clear from Figure 5 that the effect of surface tension on the measurement is not negligible and must be included in the calculated densities of molten salts. Reliable surface tension values are available in the literature for FLiNaK, but not for other salts of interest. The surface tension can be readily measured as part of the density protocol as follows. The density of any salt held at a constant temperature can be measured using nickel bobs and wires of different sizes. Because the salt density will be the same for all measurements of the same salt, the surface tension can be derived by equating values of the right-hand side of Equation 1 that are calculated using values obtained with different bobs and wires. The values of Δm , D , and V_o will differ for each measurement, but the other terms will be constant, including σ , which is the only unknown variable. Tests are in progress to demonstrate this approach and those results will be included in future reports.

3.3 Discussion of Density Measurements

The densities measured at different temperatures in 2019 and 2020 are plotted in Figure 6 alongside trends from the literature [4, 7, 8, 9]. The densities we measured are consistent with the trends given by Janz [7] and Chrenkova [4], but have lower values. The results of Vriesema et al. [8] and Powers [9] overlap in Figure 6; those values are higher and show a slightly different temperature dependency than the others. All cited references used methods based on the Archimedes principle to determine FLiNaK density. Janz [1967] and Chrenkova [2003] reported a 2% and 0.4% error while Powers [1963] and Vriesema [1979] reported a 5% error. It is likely that the lower density values reported by Janz and Chrenkova were due to neglecting the surface tension term. Neither Janz [1967] nor Chrenkova [2003] mention the surface tension effect and Janz first reported the surface tension of FLiNaK in 1988.

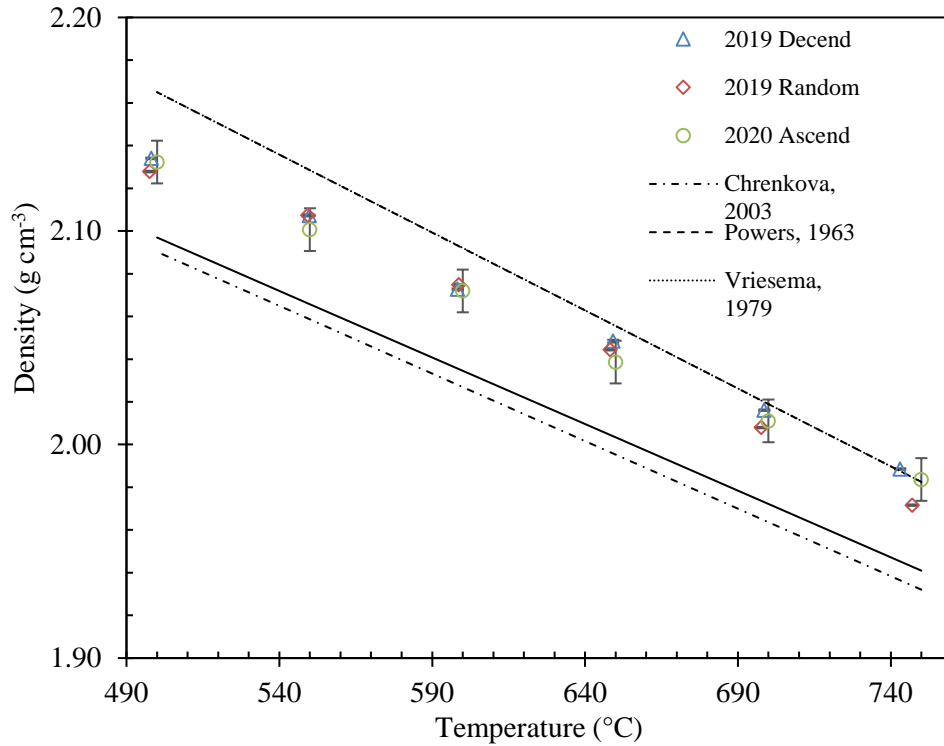


Figure 6. Measured Density of FLiNaK Compared with Literature Values [7,10,11,12]

4. Viscosity

Viscosity of molten salts is a crucial parameter for design and safety assessments of a molten salt reactor (MSR). It is needed to predict fluid flow rate and required pumping power during normal operations. It is also important when considering accident scenarios in which salt is expected to leave the primary loop and flow into a drain tank. Establishing a standard procedure for measuring the viscosity of molten salts and a reference salt to quantify the expected precision will enable measurements to be validated across laboratories, providing data with the appropriate quality for these design and safety assessments.

4.1 Viscosity Measurement Method

The viscosity of a molten salt can be measured using a rotational viscometer in which shear is applied by the rotation of a cylindrical spindle suspended in molten salt inside a container. The system measures the torque required to maintain a constant rotational speed in the fluid. This relationship is quantified in Equation 4, where viscosity (μ) is defined as the ratio of shear stress (τ) to the shear rate (γ) that can be represented in terms of the torque, rotational speed, and system parameters [3,11].

$$\mu = \frac{\tau}{\gamma} = \frac{M(R_c^2 - R_b^2)}{8\pi^2 R_c^2 R_b^2 L \left(\frac{N}{60}\right)} \quad (4)$$

In this equation, M is the torque measured by the instrument during rotation, R_b is the radius of the rotating spindle, L is the effective length of the spindle, N is the rotational speed of the spindle in revolutions per minute (rpm), and R_c is the inner radius of the container. The spindle and container are precisely sized to maintain a thin layer of fluid between the cylinder and container surface of known dimensions.

Equation 4 is only valid when flow is laminar and fully developed [3,11]. If the spindle speed is too low, the effective length of the spindle will be shortened in an unmeasurable way and using Equation 4 will provide artificially high viscosity values. If the spindle speed is too high, the flow will be turbulent and using Equation 4 will provide artificially high viscosity values. If the startup time before measurements is too short to achieve fully developed flow, then the flow will have turbulent characteristics during the measurements and lead to artificially high viscosity values. Measurements must be made at several spindle speeds to determine stable viscosity values that are least impacted by end effects or turbulence and after several startup times to confirm that conditions were appropriate to attain fully developed flow. Because end effects and turbulence both lead to artificially high viscosities being measured, the lowest viscosities determined within a series of rotational speeds and longest startup times will provide the most accurate values.

The Argonne apparatus consists of a Brookfield viscometer head that is supported on a rack and pinion stand and positioned over a benchtop Kerr furnace. A custom spindle is suspended from the head by a long drive shaft. A thermal shield is placed on top of the furnace to protect the viscometer head from temperatures over 40 °C, which would damage the instrument. The entire apparatus is housed in an inert atmosphere glovebox that maintains an atmosphere with less than 10 ppm O₂ and less than 1 ppm H₂O. The furnace is outfitted with an over-temperature shutoff and the controls are external to the glovebox. Figure 7 is a photograph of the viscometer (Brookfield Ametek, Middleboro, MA) and furnace.

A graphite crucible is used to contain the salt. Empty crucibles are heated in the Kerr furnace at 700 °C for more than 12 hours to outgas impurities prior to use. The crucible is designed to maintain the salt at a constant level in the annulus after the spindle is immersed and during the measurements. The dimensions of the spindle and graphite crucible are carefully controlled to meet the requirement that $R_c \leq 2R_b$ to attain a well-defined shear rate [3]. Spindles are washed with methanol and heated to 700 °C in an inert atmosphere for at least 12 hours to remove any surface contamination before being immersed in the salt.

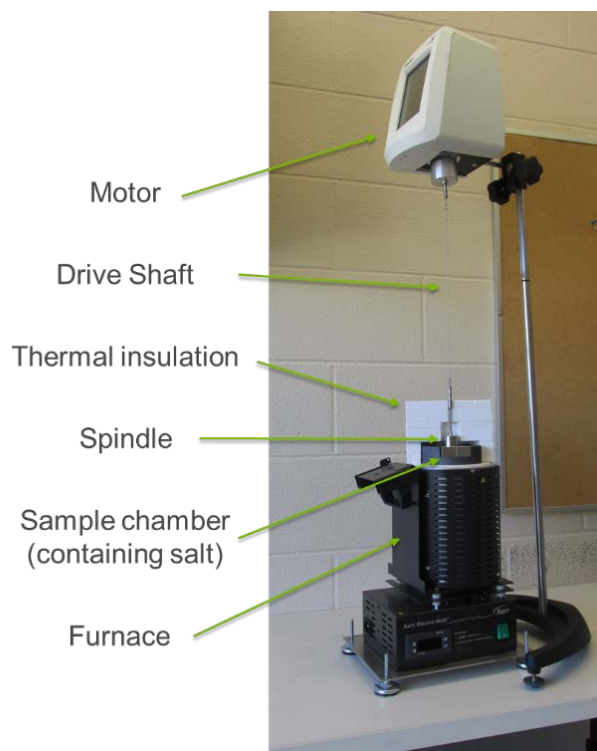


Figure 7. Photograph of Viscometer

Salts are mixed, melted, and thermally equilibrated in the crucible at 700 °C (or higher) prior to the tests. The spindle is suspended in the heated zone of the furnace above the salt level during this period to be heated before being immersed in the salt. An additional period of more than two hours is allowed after immersion for the spindle to thermally equilibrate with the salt before measurements are made. Data are taken at 25 °C intervals over the temperature range of interest (typically between 600 and 700 °C) and the molten salt and spindle are allowed to re-equilibrate for more than two hours after changing the temperature before measurements are made. In initial measurements the viscometer measured the torque at 20-second intervals over a two-minute period and provided the average and standard deviation of the six measured values. Data were collected using several spindle speeds at each temperature.

4.2 Viscosity Measurements of Eutectic FLiNaK

Viscosity of eutectic FLiNaK was measured at temperatures between about 600 and 750 °C. Figure 8 shows the viscosities measured at 650 °C using a range of spindle speeds. The viscosities represented by open symbols are affected by edge effects at the lowest speed (20 rpm), by turbulence at the highest speed (160 rpm), and impacted by insufficient startup times at intermediate speeds. All of these effects increase the calculated viscosity. The rotational speeds at which these effects are significant depend on the viscosity of the fluid and must be determined for each temperature.

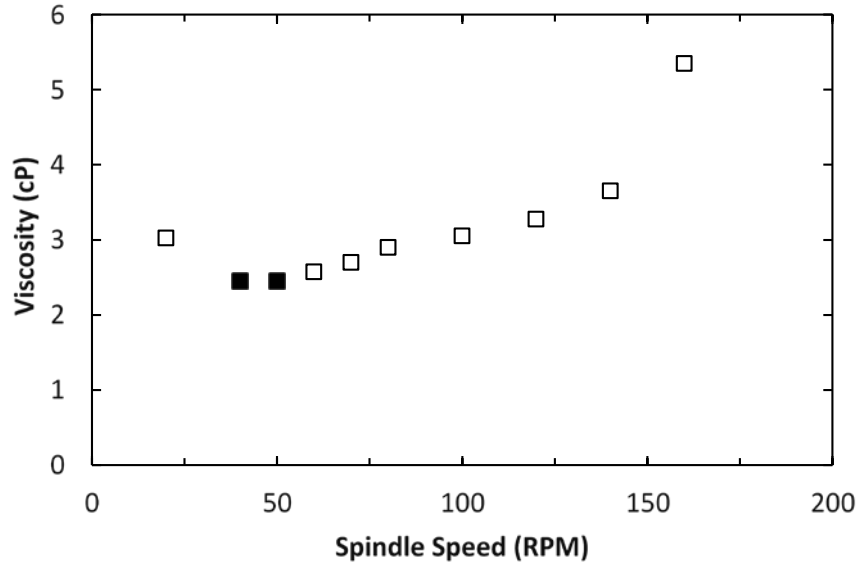


Figure 8. Measured Viscosity of FLiNaK at Different Spindle Speeds at 650 °C

The averages of viscosities determined in replicate measurements at spindle speeds of 40 and 50 rpm at each temperature are plotted in Figure 9. The error bars represent the standard deviation and a regression equation is presented for the average values. Figure 9 also shows the temperature dependencies of viscosities measured by Chrenkova [4] and by Cohen and Jones [5] for comparison. The differences between the results obtained here and those trends increase with increasing temperature. Because the effects of turbulence on the measured viscosity also increase with increasing temperature, the lower values measured here are probably more accurate.

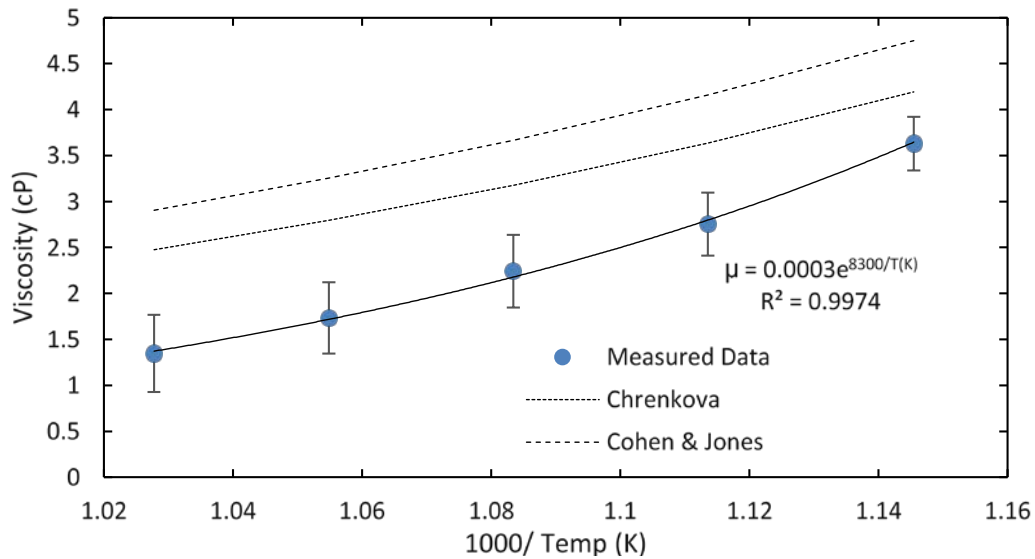


Figure 9. Measured Viscosity of FLiNaK and Literature Trends Between 600 and 750 °C

4.3 Improved Viscosity Measurement Protocol

Both the apparatus and measurement method are being modified to improve the measurement uncertainty and precision. Development of the viscosity apparatus includes improving thermal behavior through increased insulation, improving alignment of the device to reduce gyration, scaling down to decrease the required amount of salt and end effects. Development of the viscosity measurement method has focused on achieving and verifying that laminar steady state flow during operation through examining possible benefits of increasing start up time and the effects of a wider and more detailed range of spindle speeds.

For Equation 4 to be applicable, it is essential that the salt flow in the viscometer be entirely in the radial direction [3, 11]. Effective thermal insulation of the viscometer is necessary to prevent axial flow in the salt bath due to natural convection. Previously, the viscometer was insulated using two half circle pieces of RS100 insulation placed on the top of the furnace over the salt bath with a central semicircle cut out for the spindle support rod to pass through. The insulation was found to be abraded frequently during operation causing fine particles of insulation to flake off. These fine particles occasionally fell into the salt bath to contaminate the fluid and necessitated frequent changes of the salt. New insulators have been fabricated in which the RS100 is encased in stainless steel to prevent abrasion and flaking. The insulators also extend around the edge of the furnace to reduce heat loss from between the insulator and the furnace. A schematic of one side of a new insulator is shown in Figure 10.

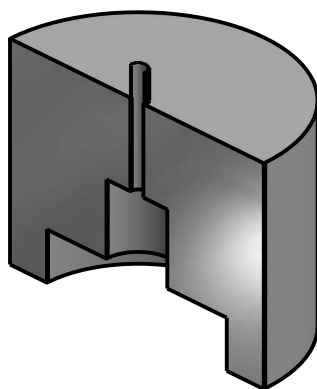


Figure 10. Half of Insulator for Viscometer

The geometries of the spindle and crucible were evaluated to assess how they affect the flow pattern of the salt during spindle rotation and could be further optimized. Figure 11 is a schematic of the spindle and crucible with relevant dimensions labeled. Eddies form around the bottom and top ends of the spindle during rotation to generate axial flow. Surveyed literature indicates that the gap between spindle and crucible should be minimized to reduce this eddy formation [11]. In order to reduce this gap, it is essential that the spindle be perfectly centered in the crucible.

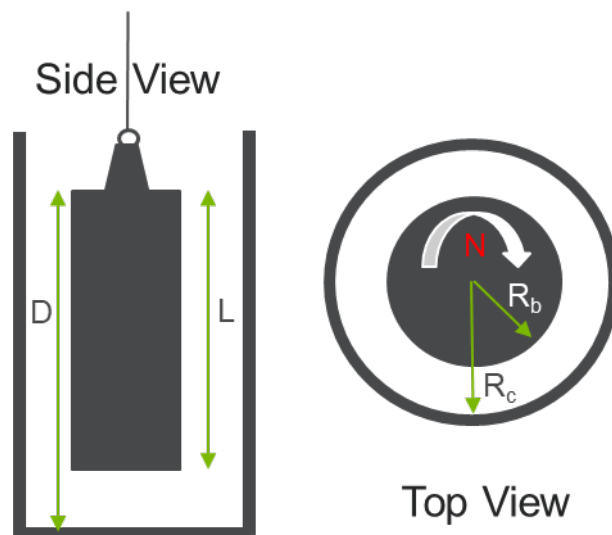


Figure 11. Schematic of Spindle in Crucible

The furnace housing the crucible has been mounted on an XY translation stage to provide fine adjustments for positioning the spindle in the center of the crucible. Prior to operation, with the thermal insulation removed, a centering disk will be placed over the top of the crucible and a pointed plumb bob will be hung from the spindle support rod while fine adjustments are made to the translation stage to center the crucible relative to the spindle. Once aligned, the centering disk will be removed and the thermal insulation installed.

Once the system is aligned, measurements will be made using three crucibles having different inner radii that provide different gaps between the crucible and spindle to determine the effect on the measured viscosity. The previous crucible-to-spindle gap was 0.318 cm and the three crucibles to be used in the test will provide 0.300 cm, 0.250 cm and 0.200 cm gaps. Quantifying the effect of the crucible-to-spindle gap may allow the apparatus to be optimized for measuring a wide range of viscosities. Reducing this gap will also decrease the volume of salt necessary to make measurements, which conveniently will enable future work using salts with higher concentrations of radionuclides.

Having optimized the gap, any remaining end effect will be determined by making measurements using spindles of different lengths [11, 5]. The measurements will be made using spindles with lengths of 3, 4, and 5 cm that vary the value of L in Equation 4.

In addition to improving the geometry of the apparatus to eliminate experimental artifacts, changes to the measurement protocol will also be made. A range of start up times will be evaluated to ascertain the minimum start up time required to achieve fully developed flow for different viscosities. For example, the variation in measured values shown in Figure 8 (including values observed at spindle speeds in non-turbulent flow regimes) indicates that the start up time of 20 seconds used for all measurements was insufficient for FLiNaK at 650 °C. Longer startup times

of 30, 40, 60 and 120 seconds will be tested. If variation in measured values at non-turbulent flow regimes persists, even longer start up times may be evaluated.

After end effects have been reduced and required start up times are determined, it may become possible to make measurements at lower spindle speeds than used previously where turbulent flow regimes are less likely to occur. A wide range of spindle speeds between 5 and 180 rpm will be examined to examine the effect of spindle speed and the resultant flow regimes. Small increments of 2-5 rpm will be used to examine the sensitivity at spindle speeds <100 rpm and large intervals of 20 rpm will be used to examine the sensitivity at higher spindle speeds.

We anticipate that optimizing the cell geometry to minimize end effects, ensuring sufficient start up time, making measurements at a range of spindle speeds that achieve fully developed laminar flow, and properly taking effects that cannot be eliminated into account will provide the most accurate measurements of viscosity possible. The extensive data based for measurements of FLiNaK will support evaluating its use as a reference material for viscosity measurements. The values measured for eutectic FLiNaK and FLiBe will be compared to available literature values for these salts.

5. Thermal Diffusivity

Thermal behavior of molten salts including the thermal diffusivity and thermal conductivity are crucial parameters for both operating an MSR and the design and safety assessments needed to obtain NRC approval. How quickly heat is transmitted through a molten salt has implications for normal operations, but becomes crucial when considering accident scenarios where salt is expected to leave the primary loop. Establishing a standard procedure for measuring the thermal diffusivity and calculating the thermal conductivity of molten salts and the expected precisions will enable measurements to be validated across laboratories, providing data with the appropriate quality for design and safety assessments of both normal operations and accident scenarios.

5.1 Thermal Diffusivity Measurement Method

Laser flash analysis is used to measure the thermal diffusivity of molten salts because of its accuracy and high throughput. The thermal conductivity of the salt is calculated by multiplying the thermal diffusivity by the density and the heat capacity, which are measured separately. For analysis of molten salts, the laser flash analyzer (LFA), a DLF1200 from TA Instruments, is operated under a purge of ultrahigh purity argon. For measurements at Argonne, each salt sample is contained in a two-piece graphite cell similar to that described by An et.al. [12]. Photos of empty sample cells machined from electrochemical grade graphite are shown in Figure 12. An assembled cell is shown at the top, an inverted top piece is shown on the bottom left, and the bottom dish is shown on the bottom right.



Figure 12. Photo of Empty Sample Cells

The cell bottoms have two 1-mm diameter holes to vent gas generated as the salt is heated. The cells are heated in an inert atmosphere to eliminate possible contamination of samples from the binder or machining fluids before use. The LFA provides a pulse (also referred to as a shot) from a Nd glass laser with a duration of 300-400 μs and an intensity up to 25 J to the bottom of the crucible and monitors the temperature of the top of the crucible over time. The detector unit is an indium antimonide infrared detector cooled with liquid nitrogen. The detector performance is monitored continuously during measurements by the FlashLine software. If the detector performance does not meet operational criteria, the software rejects the shot data and tries again.

A salt sample of approximately 0.75 mL is loaded into the cell inside a glovebox maintained at less than 10 ppm oxygen and less than 1 ppm moisture and melted to coalesce and degas. The sample is then cooled and packaged for transport to the LFA, where it is loaded quickly into the sample holder. Shots are typically taken at 25 $^{\circ}\text{C}$ intervals as the sample is heated. Data analysis is performed automatically by the FlashLine PostAnalysis Software, which is a TA Instruments product. The software uses the Clark and Taylor model [13] for calculating thermal diffusivity from the pulse response data. The performance of the LFA is checked periodically by using molybdenum and stainless steel standards. Figure 13 shows that the results for a representative analyses of the molybdenum standard fall within the acceptable range recommended by the manufacturer over a wide temperature range. Results from these molybdenum analyses to check instrument performance are tabulated in Appendix B, Table B.4.

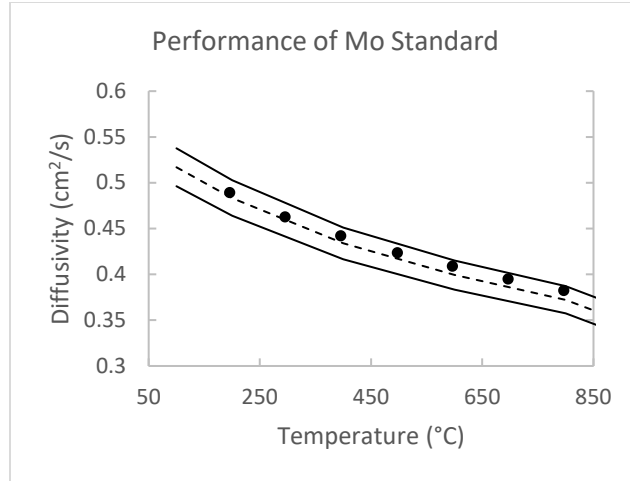


Figure 13. Results of Analyses of a Molybdenum Standard

5.2 Thermal Diffusivity of Graphite

Three samples of JC3 grade graphite were analyzed for thermal diffusivity to determine its effect on the results from analyses of molten salts in the LFA. This graphite material, purchased from Becker Brothers Corp., is machined into sample cells used to contain molten salts in the LFA. In the LFA cells shown in Figure 12, two layers of 0.5mm thick graphite are used to sandwich the salt sample between them. It is essential to understand whether these layers of graphite contribute to the measured thermal diffusivity of the salts contained inside. Currently, the effect of the graphite on the measurement is neglected and it is assumed that the heat transfer phenomena is dominated by the molten salt. This assumption is valid only if the thermal diffusivity of the salt is significantly lower than that of the graphite.

The three samples of the graphite were machined from a stock 1.25 in. diameter rod to produce specimens 1.0, 1.5 and 2.0 mm thick and 1 in. in diameter. The LFA was programmed with a ramp rate of 15 K/min and took four shots at each of four temperatures, 400, 500, 600 and 700 °C. This program was run twice for each graphite sample and each power setting. Three power settings were used for measurements with the largest sample to examine the effect of the power on the measurement. The usual unitless power setting for molten salt samples in the instrument is 1200, as recommended by the manufacturer. The use of power levels 1200, 1000 and 900 was evaluated. The LFA software used the Clark and Taylor method of determining thermal diffusivity from the temperature response of the samples, as is done to analyze the results of measurements with molten salt samples [13]. This method applies a correction for radiative heat losses to the environment.

The response to shots taken with the thinnest sample (1.0 mm) were unreadable by the LFA. This is probably because the transmission was faster than the detector could measure. The raw data for measurements with the 1.5 mm and 2.0 mm samples are shown in Appendix B, Table B.5. The

average diffusivity for the eight measurements made at each power level, thickness and temperature and one standard deviation are summarized in Table 4.

Table 4. Thermal Diffusivity Measurements of Two Graphite Samples

Thickness	Power Setting	Temperature	Diffusivity	Std. Dev.
mm	dimensionless	°C	cm²/s	cm²/s
1.5	1200	400	0.362	0.004
		500	0.297	0.005
		600	0.257	0.003
		700	0.229	0.003
2.0	900	400	0.345	0.002
		500	0.298	0.002
		600	0.263	0.002
		700	0.237	0.001
2.0	1000	400	0.346	0.003
		500	0.298	0.002
		600	0.264	0.001
		700	0.237	0.001
2.0	1200	400	0.344	0.002
		500	0.298	0.002
		600	0.264	0.001
		700	0.237	0.001

The results for shots taken at the thickest 2.0 mm samples at three power levels are shown in Figure 14. The data points are averages of the eight measurements made at each power level and temperature and the uncertainty bars represent one standard deviation. The maximum variability of diffusivity with power level occurred at 400 °C and is shown in the inset in the figure. No trend with power level is seen and the variation in the data is <1% of the measured value.

Heat is conducted by two mechanisms in conductive solids such as graphite—lattice vibrations and the movement of electrons. Lattice vibrations are an inherently slower heat transfer mechanism and electron movement is inherently faster. Heat conduction at low temperatures is dominated by the free movement of electrons and tends to increase with temperature until a critical value is reached. At temperatures above this critical value, the increased lattice vibrations begin to impede the free movement of the electrons and decrease the thermal diffusivity. As expected for a conductive solid at high temperature, Figure 14 shows the measured diffusivity of the graphite decreases with temperature.

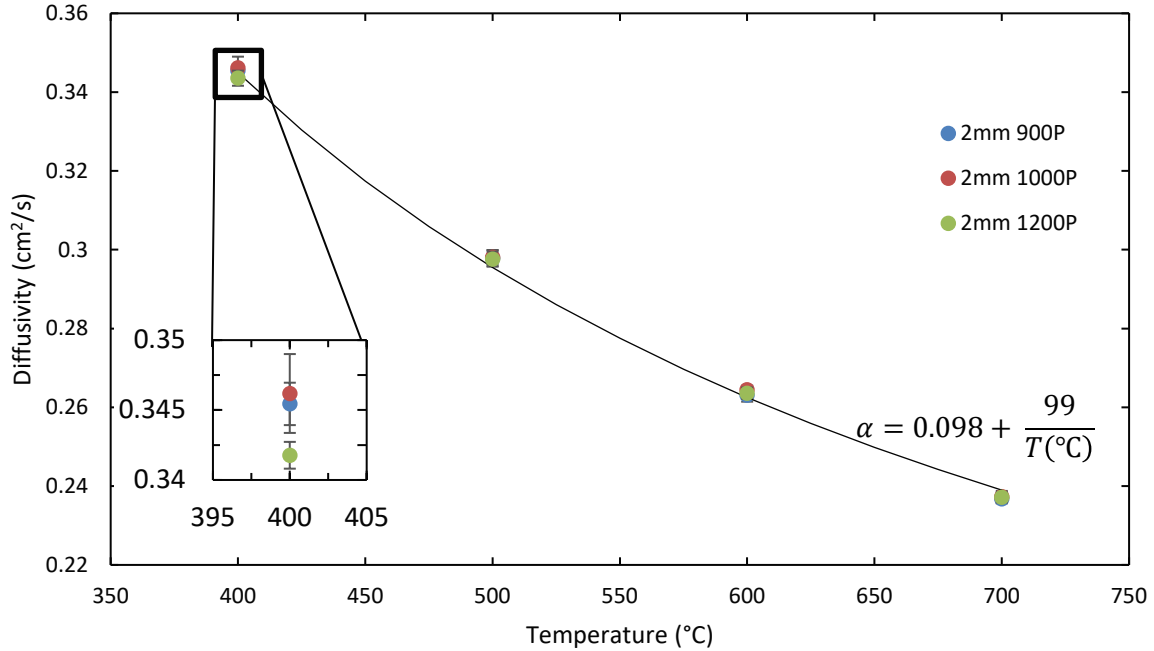


Figure 14. Thermal Diffusivity of 2mm Graphite at Three Power Settings

The curve shown in Figure 14 is fitted to the data at the 1200 power level that is usually used for molten salt measurements. The function used to fit the line is a simple rational function of the form $a+b/T$. The function constants and their standard errors are $a = 0.098 \pm 0.006 \text{ cm}^2/\text{s}$ and $b = 99 \pm 3 \text{ cm}^2\text{C}/\text{s}$.

Figure 15 shows data for analyses of the 1.5 mm and 2.0 mm thick samples at the 1200 power level. The data points are averages of the eight measurements made at each temperature for each sample and the uncertainty bars represent one standard deviation of those eight data points. The data for the 1.5 mm sample had a higher level of variability than that for the 2.0 mm sample. This could indicate that the response time for the thinner sample was approaching the minimum response time of the detector, resulting in reduced precision. This is likely because the 1.0 mm sample response time was too fast to be detected.

The analysis of very thin samples of the graphite used to construct LFA cells indicated the thermal diffusivity was at the limit of detection of the LFA. This finding is significant because the LFA cells used to contain molten salt samples consist of two layers of 0.5 mm thick graphite that sandwich the salt sample between them. The laser pulse must pass through 1.0 mm of graphite as well as the molten salt sample in each measurement. These experiments show that 1.0 mm of this graphite material transmits heat from the laser pulse faster than can be detected. This justifies neglecting the effect of the graphite on the molten salt sample measurements, as the effect is immeasurably small. These results are consistent with previous measurements made with a different type of graphite [14].

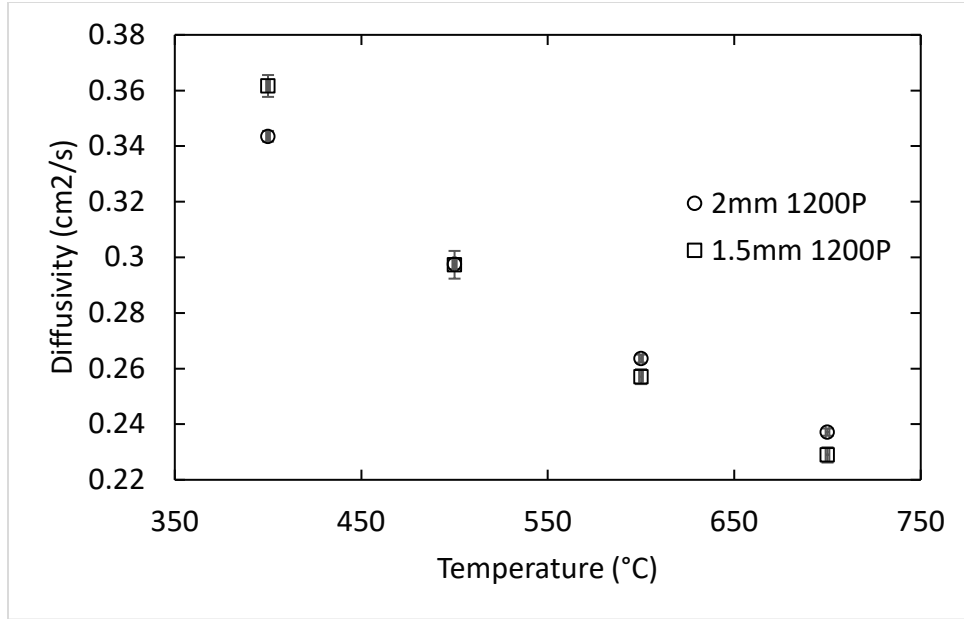


Figure 15. Thermal Diffusivity of Two Thicknesses of JC3 Graphite

5.3 Thermal Diffusivity Measurements of Eutectic FLiNaK

Figure 16 shows the results of thermal diffusivity measurements for eutectic FLiNaK (symbols) compared with a correlation published by Smirnov et al. [15] that has been converted to thermal diffusivity (line). Smirnov et al. reported an estimated error of 4%. Our data are consistent with that of Smirnov et al. within that uncertainty and the repeatability in replicate measurements is within the size of the symbol. Raw data can be found in Appendix B, Table B.6.

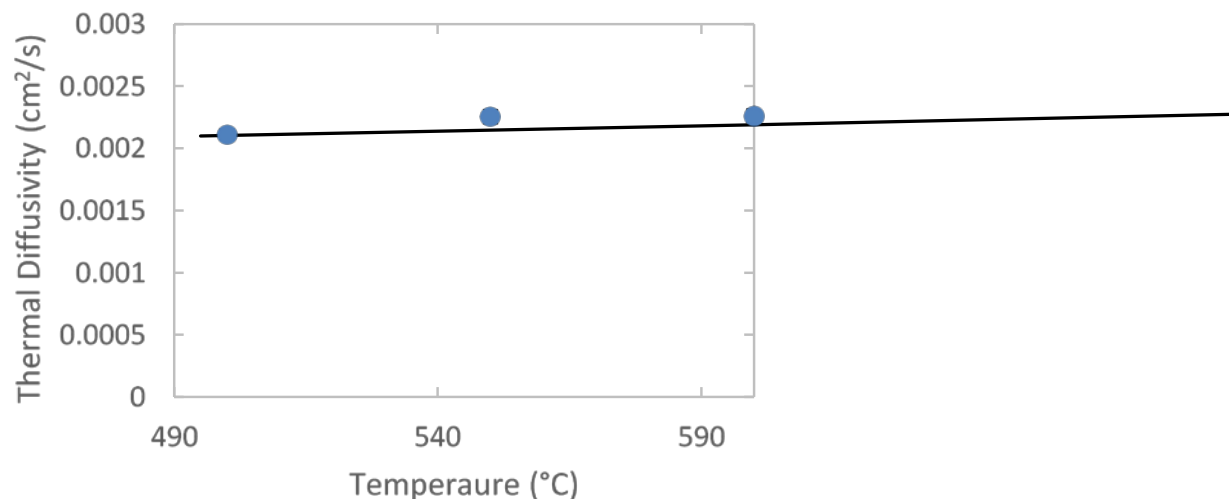


Figure 16: Measured Thermal Diffusivity of FLiNaK

The thermal diffusivity of FLiNaK at 600 °C is 0.0021 cm²/s while that of the 1.0 mm of graphite used to contain the salt is 0.26 cm²/s at 600 °C, a factor of approximately 100 larger. The effect of the graphite on the measurements of molten salt diffusivity is so small that the instrument cannot measure it. Therefore the diffusivities reported by the instrument are considered representative of the diffusivity of the molten salt alone. The maximum variation in the measured diffusivity of FLiNaK is 0.0001 cm²/s.

6. Summary

Thermophysical property measurement methods are being refined and apparatuses are being improved to provide reliable results. This work has focused on density, viscosity, and thermal diffusivity measurement methods used at Argonne. Establishment of standard procedures and expected precisions using a reference salt such as FLiNaK will enable inter-laboratory validation of molten salt property measurements in support of molten salt reactor developers.

Density measurements made with two batches of eutectic FLiNaK showed excellent repeatability over the temperature range 500–750 °C. Measurements made with two different batches and two different apparatuses demonstrated the importance of temperature control in reducing uncertainty in the calculated density values. Including the effect of surface tension on the measurements was shown to be necessary to calculate correct density values. With those corrections, measurements made using different batches were in excellent agreement. Literature values were used for the surface tension of FLiNaK, but the surface tension of other salts can be measured as part of the density measurements by using different sizes of bobs and wires. Those measurements are being included in the measurement protocol.

Viscosity measurements of eutectic FLiNaK were shown to be affected by several experimental artifacts. Work is in progress to eliminate, minimize, or quantify these experimental artifacts to reduce uncertainty and increase precision of viscosity measurements. This will lead to an optimized standard procedure for viscosity measurements using a rotational viscometer.

Thermal diffusivity measurements of FLiNaK were used to demonstrate the sensitivity and achievable precision of the laser flash technique. The procedure for preparing molten salt samples for thermal diffusivity measurements was detailed. The thermal diffusivity of the graphite from which sample containment cells are constructed for use in the LFA was measured and the effect of the graphite on the measurement of molten salts determined to be immeasurably small.

The extensive data set being generated with eutectic FLiNaK will support its use as a standard material for density, viscosity, and thermal diffusivity measurements.

Acknowledgement

This work was conducted under the auspices of DOE Advanced Reactor Technologies Molten Salt Reactors campaign and is issued to meet program milestone M3AT-20AN040601084.

This work was conducted at Argonne National Laboratory and supported by the U.S. Department of Energy, Office of Nuclear Energy, under Contract DE-AC02-06CH11357.

References

- [1] M.A. Rose, E. Wu, T. Lichtenstein and J. Krueger. "Salt Production and Analysis in Support of the MSR Campaign". ANL/CFCT-20/10. March 31, 2020.
- [2] M.A. Rose, E. Wu, T. Lichtenstein and J. Krueger. "Analytical Results for FLiNaK". *Issued to University of Illinois at Urbana-Champaign under the ARPA-E Meitner Program*. Sept. 15, 2020.
- [3] AMETEK Brookfield, Inc. "More Solutions to Sticky Problems" Instrumentation and Specialty Controls Division. Middleboro, MA. 2017.
- [4] M. Chrenkova, V. Danek, R. Vasiljev, A. Silny, V. Kremenetsky and E. Polyakov. "Density and Viscosity of the $(\text{LiF-NaF-KF})_{\text{eut}}-\text{KBF}_4\text{-B}_2\text{O}_3$ Melts". *Journal of Molecular Liquids* **102** (1-3) 213-226. 2003.
- [5] S. Cohen and T. Jones. "Viscosity Measurements on Molten Fluoride Mixtures". ORNL-2278. *Aircraft Reactor Engineering Division*. Contract No. W-7405-eng-26. 1957.
- [6] S. W. Hughes, "Measuring liquid density using Archimedes' Principle," *Physics Education* **41** 445 (2006). <http://iopscience.iop.org/article/10.1088/0031-9120/41/5/011/meta>
- [7] Janz G.J., 1967 "Thermodynamic and Transport Properties for Molten Salts: Correlation Equations for Critically Evaluated Density, Surface Tension, Electrical Conductance and Viscosity Data". *Journal of Physical and Chemical Reference Data*, 17(2), 1.
- [8] Vriesema, I.B., "Aspects of Molten Fluorides as Heat Transfer Agents for Power Generation". *Delft University of Technology*, Delft, Netherlands. Report WTHD No. 112. 1979.
- [9] Powers W. D., Cohen S. I. and Greene N. D. "Physical Properties of Molten Reactor Fuels and Coolants" *Nuclear Science and Engineering*, 17(2) 200-211 (1963)
- [10] Janz, George J. "Thermodynamic and transport properties for molten salts: correlation equations for critically evaluated density, surface tension, electrical conductance, and viscosity data." *Journal of Physical and Chemical Reference Data* 17 (1988).
- [11] Lindsey, C.H. and Fischer, E.K. "End Effect in Rotational Viscometers". *Journal of Applied Physics*. **18** 988, 1947.
- [12] Xue-Hui An, Jin-Hui Cheng, Hui-Qin Yin, Lei Dong Xie and Peng Zhang. "Thermal Conductivity of High Temperature Fluoride Molten Salt Determined by Laser Flash Technique". *International Journal of Heat and Mass Transfer*. **90**. p872-877 (2015)
- [13] Data Sheet on LFA
- [14] McEligot, D.M., Swank, W.D., Cottle, D.L and Valentin, F.I. "Thermal Properties of G-348 Graphite". Idaho National Laboratory and City College of New York. May 2016. INL/EXT-16-38241
- [15] M.V. Smirnov, V.A. Khokhlov and E.S. Filatov. "Thermal Conductivity of Molten Alkali Halides and their Mixtures". *Electrochimica Acta* 32(7) 1019-1026. 1987.

Appendix A: Material Certificates for Salt Reagents

Figure A.1 Certificate of Analysis for LiF



Specification

1.05686.0050 Lithium fluoride 99.99 Suprapur®

Specification		
Purity (metallic)	≥ 99.99	%
Ba (Barium)	≤ 5.0	ppm
Ca (Calcium)	≤ 2.0	ppm
Cd (Cadmium)	≤ 0.5	ppm
Co (Cobalt)	≤ 0.5	ppm
Cs (Cesium)	≤ 20	ppm
Cu (Copper)	≤ 0.5	ppm
Fe (Iron)	≤ 0.5	ppm
K (Potassium)	≤ 10	ppm
Mg (Magnesium)	≤ 0.5	ppm
Mn (Manganese)	≤ 0.5	ppm
Na (Sodium)	≤ 10	ppm
Ni (Nickel)	≤ 0.5	ppm
Pb (Lead)	≤ 0.5	ppm
Rb (Rubidium)	≤ 10	ppm
Sr (Strontium)	≤ 5	ppm
Zn (Zinc)	≤ 0.5	ppm

Evelyn Allmann

Responsible laboratory manager quality control

This document has been produced electronically and is valid without a signature.

Figure A.2 Certificate of analysis for NaF.

SIGMA-ALDRICH®

sigma-aldrich.com

3050 Spruce Street, Saint Louis, MO 63103, USA

Website: www.sigmaaldrich.com

Email USA: techserv@sial.com

Outside USA: eurtechserv@sial.com

Certificate of Analysis

Product Name:

Sodium fluoride – anhydrous, powder, 99.99% trace metals basis

Product Number:

450022

Batch Number:

MKBV9645V

Brand:

ALDRICH

CAS Number:

7681-49-4

MDL Number:

MFCD00003524

Formula:

FNa

Formula Weight:

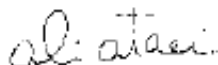
41.99 g/mol

Quality Release Date:

17 JUL 2015

NaF

Test	Specification	Result
Appearance (Color)	White	White
Appearance (Form)	Powder	Powder
Gravimetric Analysis		45.3 %
% F With Lead Acetate		
ICP Major Analysis	Confirmed	Conforms
Confirms Sodium Component		
Purity	Meets Requirements	Meets Requirements
99.99% Based On Trace Metals Analysis		
Trace Metal Analysis	≤ 150.0 ppm	31.3 ppm
Aluminum (Al)		0.6 ppm
Barium (Ba)		0.5 ppm
Calcium (Ca)		1.5 ppm
Cesium (Cs)		5.0 ppm
Iron (Fe)		14.2 ppm
Potassium (K)		6.6 ppm
Lithium (Li)		0.9 ppm
Magnesium (Mg)		1.3 ppm
Manganese (Mn)		0.3 ppm
Rubidium (Rb)		0.4 ppm
Strontium (Sr)		< 0.1 ppm



Ali Ataei, Manager

Figure A.3 Certificate of analysis for KF.

SIGMA-ALDRICH®

sigma-aldrich.com

3050 Spruce Street, Saint Louis, MO 63103, USA

Website: www.sigmaaldrich.comEmail USA: techserv@sial.comOutside USA: eurtechserv@sial.com**Certificate of Analysis**

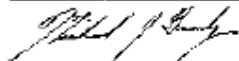
Product Name:

Potassium fluoride – anhydrous, powder, ≥99.9% trace metals basis

Product Number: 449148
Batch Number: MKBX2566V
Brand: ALDRICH
CAS Number: 7789-23-3
MDL Number: MFCD00011398
Formula: FK
Formula Weight: 58.10 g/mol
Quality Release Date: 31 DEC 2015

KF

Test	Specification	Result
Appearance (Color)	White	White
Appearance (Form)	Powder	Powder
ICP Major Analysis	Confirmed	Confirmed
Confirms K Component		
Purity	Conforms	Conforms
≥99.9% Based On Trace Metals Analysis		
Trace Metal Analysis	≤ 1000.0 ppm	614.7 ppm
Boron (B)		1.4 ppm
Calcium (Ca)		3.0 ppm
Chromium (Cr)		2.1 ppm
Cesium (Cs)		12.7 ppm
Iron (Fe)		8.4 ppm
Lithium (Li)		1.9 ppm
Manganese (Mn)		0.9 ppm
Sodium (Na)		527.4 ppm
Rubidium (Rb)		57.0 ppm



Michael Grady, Manager
 Quality Control
 Milwaukee, WI US

Appendix B: Data

Table B.1. Mass Measurements of Bob Submerged in 2019, random order FLiNaK Salt^a

T (°C)	497.6	549.3	598.8	648.2	697.6	747.1
Mass (g)	3.298	3.305	3.318	3.330	3.345	3.360
	3.298	3.305	3.318	3.330	3.345	3.360
	3.298	3.305	3.318	3.330	3.345	3.360
	3.298	3.305	3.318	3.330	3.345	3.360
	3.297	3.304	3.317	3.331	3.344	3.361
	3.299	3.306	3.319	3.329	3.346	3.359

^aMass in glovebox atmosphere = 4.21 g.

Table B.2. Mass Measurements of Bob Submerged in 2019, descend order FLiNaK Salt^a

T (°C)	498.2	549.9	598.3	649.2	698.6	743.1
Mass (g)	3.295	3.305	3.319	3.331	3.341	3.352
	3.295	3.305	3.319	3.330	3.341	3.352
	3.295	3.305	3.319	3.328	3.341	3.352
	3.295	3.305	3.319	3.329	3.341	3.352
	3.294	3.304	3.318	3.328	3.342	3.351
	3.296	3.306	3.320	3.329	3.340	3.353

^aMass in glovebox atmosphere = 4.21 g.

Table B.3. Mass Measurements of Bob Submerged in 2020, ascend order FLiNaK Salt^a

T (°C)	500	550	600	650	700	750
Mass (g)	14.247	14.271	14.362	14.402	14.412	14.502
	14.243	14.291	14.328	14.419	14.433	14.512
	14.250	14.320	14.314	14.447	14.463	14.550
	14.238	14.310	14.335	14.382	14.470	14.478
	14.244	14.271	14.316	14.397	14.469	14.456
	14.220	14.296	14.338	14.414	14.465	14.507
	14.254	14.300	14.375	14.428	14.512	14.535
	14.230	14.270	14.366	14.454	14.486	14.495
	14.247	14.312	14.363	14.385	14.437	14.482
	14.236	14.326	14.346	14.401	14.479	14.491
	14.231	14.299	14.351	14.375	14.455	14.472
	14.224	14.288	14.368	14.416	14.472	14.506
	14.228	14.276	14.375	14.433	14.489	14.493
	14.224	14.288	14.371	14.442	14.472	14.511
	14.241	14.314	14.332	14.404	14.412	14.502
	14.215	14.274	14.316	14.375	14.462	14.533
	14.230	14.315	14.349	14.386	14.423	14.526
	14.234	14.290	14.342	14.406	14.445	14.553
	14.236	14.272	14.325	14.380	14.432	14.537
	14.230	14.273	14.330	14.399	14.466	14.496

^aMass in glovebox atmosphere = 18.48 g.

Table B.4. Raw Thermal Diffusivity Measurements of the Molybdenum Standard Material

Test #	T(°C)	Avg.	Std. Dev.	Thermal Diffusivity (cm ² /s)									
				Shots									
1	99	0.522	4.79E-03	0.5169	0.5263	0.5232							
	198	0.488	1.35E-03	0.4894	0.4879	0.4867							
	291	0.462	2.93E-03	0.4645	0.4590	0.4635							
	396	0.444	2.65E-04	0.4438	0.4439	0.4434							
2	99	0.524	1.12E-03	0.5238	0.5254	0.5234	0.5240	0.5249	0.5238	0.5212	0.5245	0.5235	0.5240
	198	0.489	6.58E-04	0.4903	0.4903	0.4902	0.4890	0.4886	0.4893	0.4891	0.4895	0.4886	0.4891
	294	0.464	9.32E-04	0.4652	0.4643	0.4650	0.4619	0.4646	0.4641	0.4634	0.4643	0.4641	0.4645
	397	0.443	6.24E-04	0.4435	0.4427	0.4435	0.4441	0.4436	0.4429	0.4427	0.4420	0.4425	0.4432
	499	0.424	2.22E-03	0.4257	0.4252	0.4184	0.4244	0.4248	0.4246	0.4245	0.4266	0.4248	0.4253
	598	0.410	7.56E-04	0.4101	0.4104	0.4079	0.4101	0.4097	0.4105	0.4103	0.4099	0.4098	0.4104
3	386	0.444	6.56E-04	0.4451	0.4443	0.4438							
	496	0.426	7.77E-04	0.4267	0.4256	0.4252							
	597	0.410	3.06E-04	0.4096	0.4100	0.4102							
	697	0.397	5.69E-04	0.3961	0.3972	0.3964							
	796	0.384	1.73E-04	0.3837	0.3837	0.3834							
4	196	0.489	1.18E-03	0.4905	0.4882	0.4889							
	296	0.463	2.00E-04	0.4626	0.4628	0.4624							
	396	0.442	6.81E-04	0.4414	0.4427	0.4417							
	498	0.424	5.77E-04	0.4238	0.4238	0.4228							
	597	0.409	1.03E-03	0.4099	0.4079	0.4085							
	697	0.395	1.15E-04	0.3948	0.3948	0.3950							
	797	0.382	4.16E-04	0.3826	0.3818	0.3820							
5	387	0.442	2.52E-04	0.4421	0.4426	0.4423							
	498	0.423	1.53E-04	0.4230	0.4229	0.4232							
	597	0.407	3.44E-03	0.4028	0.4086	0.4089							
	697	0.398	4.42E-03	0.3954	0.4029	0.3951							

Table B.5. Raw Thermal Diffusivity Data from Measurements of JC3 Graphite

Run Details	Temp. °C	Raw Thermal Diffusivity Measurements			
		cm ² /s			
2mm, 900 power level, Run 1	400	0.347	0.346	0.346	0.348
	500	0.299	0.302	0.297	0.297
	600	0.264	0.263	0.264	0.265
	700	0.238	0.238	0.237	0.238
2mm, 900 power level, Run 2	400	0.344	0.345	0.344	0.344
	500	0.297	0.298	0.295	0.298
	600	0.262	0.265	0.261	0.261
	700	0.236	0.236	0.234	0.237
2mm, 1000 power level, Run 1	400	0.348	0.348	0.350	0.345
	500	0.299	0.298	0.299	0.300
	600	0.265	0.266	0.266	0.264
	700	0.238	0.235	0.238	0.240
2mm, 1000 power level, Run 2	400	0.345	0.349	0.344	0.342
	500	0.297	0.299	0.297	0.295
	600	0.264	0.264	0.263	0.263
	700	0.237	0.238	0.236	0.237
2mm, 1200 power level, Run 1	400	0.345	0.345	0.345	0.345
	500	0.299	0.300	0.299	0.299
	600	0.265	0.265	0.265	0.265
	700	0.238	0.238	0.237	0.239
2mm, 1200 power level, Run 2	400	0.342	0.342	0.342	0.342
	500	0.296	0.296	0.296	0.296
	600	0.262	0.262	0.262	0.263
	700	0.236	0.237	0.237	0.235
1.5mm, 1200 power level, Run 1	400	0.358	0.358	0.357	0.358
	500	0.293	0.292	0.292	0.294
	600	0.255	0.254	0.253	0.257
	700	0.226	0.227	0.226	0.226
1.5mm, 1200 power level, Run 2	400	0.365	0.366	0.366	0.364
	500	0.302	0.302	0.301	0.303
	600	0.259	0.260	0.259	0.259
	700	0.231	0.232	0.232	0.231

Table B.6. Raw Thermal Diffusivity Data for FLiNaK

Run #	T (°C)	Diffusivity (cm ² /s)						
		Average	Std. Dev.	Shots				
1	495	2.1E-03	0.0E+00	0.0021	0.0021	0.0021		
	549	2.2E-03	5.8E-05	0.0023	0.0022	0.0022		
	599	2.3E-03	0.0E+00	0.0023	0.0023	0.0023		
2	545	2.2E-03	5.8E-05	0.0022	0.0023	0.0022	0.0023	0.0022
	599	2.2E-03	5.8E-05	0.0022	0.0023	0.0023	0.0023	0.0022
3	495	2.1E-03	5.8E-05	0.0021	0.0021	0.0022	0.0021	0.0021
	549	2.3E-03	5.8E-05	0.0023	0.0023	0.0023	0.0023	0.0022
	599	2.2E-03	5.8E-05	0.0023	0.0022	0.0023	0.0022	0.0022



Chemical and Fuel Cycle Technologies Division

Argonne National Laboratory
9700 South Cass Avenue, Bldg. 205

Argonne, IL 60439

www.anl.gov



U.S. DEPARTMENT OF
ENERGY

Argonne National Laboratory is a U.S. Department of Energy
laboratory managed by UChicago Argonne, LLC